

# Evaporation induced self-assembly of different shapes and sizes of nanoparticles: A molecular dynamics study

Cite as: J. Chem. Phys. 150, 044708 (2019); <https://doi.org/10.1063/1.5053974>

Submitted: 28 August 2018 . Accepted: 14 December 2018 . Published Online: 30 January 2019

Parul Katiyar, and Jayant K. Singh



View Online



Export Citation



CrossMark

## ARTICLES YOU MAY BE INTERESTED IN

[Molecular dynamics simulations of evaporation-induced nanoparticle assembly](#)

The Journal of Chemical Physics **138**, 064701 (2013); <https://doi.org/10.1063/1.4789807>

[Evaporation-induced assembly of colloidal crystals](#)

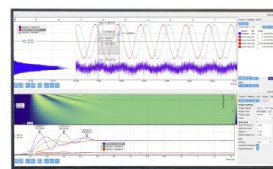
The Journal of Chemical Physics **149**, 094901 (2018); <https://doi.org/10.1063/1.5043401>

[Formation of coffee-stain patterns at the nanoscale: The role of nanoparticle solubility and solvent evaporation rate](#)

The Journal of Chemical Physics **146**, 114503 (2017); <https://doi.org/10.1063/1.4978284>

Challenge us.

What are your needs for  
periodic signal detection?



Zurich  
Instruments



# Evaporation induced self-assembly of different shapes and sizes of nanoparticles: A molecular dynamics study

Cite as: J. Chem. Phys. 150, 044708 (2019); doi: 10.1063/1.5053974

Submitted: 28 August 2018 • Accepted: 14 December 2018 •

Published Online: 30 January 2019



View Online



Export Citation



CrossMark

Parul Katiyar and Jayant K. Singh<sup>a)</sup>

## AFFILIATIONS

Department of Chemical Engineering, Indian Institute of Technology Kanpur, Kanpur 208016, India

<sup>a)</sup> Author to whom correspondence should be addressed: [jayantks@iitk.ac.in](mailto:jayantks@iitk.ac.in). Telephone: 91-512-259 6141. Fax: 91-512-259 0104.

## ABSTRACT

Molecular dynamics simulations of Lennard-Jones particles have been performed to study the self-assembled structure of nanoparticles (NPs) formed upon evaporation of nanofluid droplets on a heated surface. Different shapes of NPs such as a sphere, cube, triangle, and rod are considered in this work for the nanofluid. The influence of solvent-surface and NP-surface interaction strengths, size, and shape of NPs is analyzed on the structure of the NP deposit formed upon evaporation. The solvophilic substrate leads to the formation of different structures such as the hemispherical clump, monolayer, and ring depending on the size, shape, and interaction between other pairs of atoms. On the other hand, the solvophobic substrate always leads to a clump of NPs. Structural and thermodynamic properties are calculated to characterize the self-assembled structures. The low pair energy and high excess entropy are the characteristics of a ring structure. Furthermore, the mean square displacement of NPs is found to be lower for the ring structure compared to the hemispherical clump structure, and this observation is independent of the shape and size of the NP. The change in arrangement from disorder to order is observed for rod shaped NPs during evaporation.

Published under license by AIP Publishing. <https://doi.org/10.1063/1.5053974>

## I. INTRODUCTION

Evaporation is a spontaneous phenomenon which has many industrial applications such as heat transfer, printing,<sup>1,2</sup> cooling, drying, and coating. Evaporation also finds technological applications in fabrication of optical and electronic devices,<sup>3</sup> inkjet printing,<sup>4</sup> developing low-cost technologies for disease diagnostics in resource-poor environments,<sup>5</sup> preparing coatings for the retinal implants,<sup>6</sup> and preparation of Janus particles.<sup>7,8</sup> Evaporation induced self-assembly can be combined smoothly with micrometer-scale film patterning schemes such as lithography, microcontact printing, and direct writing. Evaporation is one of the simplest methods to assemble nonvolatile solutes into complex structures on different scales.<sup>9</sup>

It is known that adding nanoparticles (NPs) to the fluid influences the evaporation rate.<sup>10,11</sup> Depending on the type of NP, the evaporation rate gets enhanced or slowed down.

Evaporation of nanofluid leads to the formation of self-assembled structures of NPs which find use in various applications, depending on the shape of the structure formed. For example, high-resolution inkjet printing of conductive carbon nanotubes in water leads to the formation of conductive twin line tracks due to the coffee-ring effect.<sup>4</sup> The formation of a coffee-ring during evaporation shows the ability to separate particles based on their size.<sup>5</sup> Formation of uniform coating<sup>12</sup> and a clump is useful in printing. Evaporation also leads to better dispersion of nanoparticles in a polymer film having weak NP/polymer interactions opposite to the general belief that strong NP/polymer attractions are required to make NPs disperse well in polymer nanocomposites.<sup>13</sup>

It is observed that the structure of the deposit can vary depending on the nanofluids, substrate/geometry, and evaporating rate. For instance, ring-like patterns are formed by silver NPs on the glass surface during drying,<sup>14</sup> the periodic parallel array of nanopillars and nanoholes is formed by

geometrically confined evaporative self-assembly,<sup>15</sup> and a highly ordered NP monolayer is formed by attractive NPs under fast evaporation conditions.<sup>12</sup> The shape of the deposit formed by evaporation can be modified by changing some of the conditions. For example, the shape of the deposit formed after evaporating nanofluid containing titania NPs on a glass substrate changes from ring-like to uniform with pH.<sup>16</sup> This is mainly due to the change in the DLVO (Derjaguin, Landau, Verwey, and Overbeek) interactions with changes in the pH values. The temperature of the substrate also affects the pattern formed by a volatile drop.<sup>17</sup> For a strongly pinned fluid, the smaller size NPs uniformly cover the entire wet area of the drop, while the larger size NPs lead to the deposition of NPs at the rim of the droplet displaying the coffee-ring effect.<sup>18</sup> It is also observed that the addition of another component along with the NPs leads to a change in the surface pattern formed.<sup>19–21</sup> The coffee-ring effect is suppressed by the drop casting of the hybrid solution of graphene oxide and monolayer titania 2D sheets<sup>19</sup> as compared to the solution of individual components due to the strong interaction between the graphene and titania. A silicone oil coating on a glass substrate also helps in suppressing the coffee-ring effect.<sup>20</sup> The surfactant also affects the self-assembled structure. An addition of the cetyl tri methyl ammonium bromide (CTAB) surfactant to graphite NPs solution leads to the formation of a coffee-ring as compared to the uniform coating without a surfactant.<sup>21</sup> Changing the evaporation rate also changes the formed pattern, and lowering the evaporation rate leads to the coffee-ring effect from a uniform deposition.<sup>22</sup>

The surface nature plays an important role in the final structure observed in these studies. Hydrophilic surfaces are more amicable to yield different structures as discussed above, while hydrophobic surfaces in general lead to the formation of a clump of NPs.<sup>23</sup> For example, in the case of a silane modified glass surface with increasing hydrophobicity, a uniform clump of biomolecules is formed.<sup>24</sup> Pattern formation on hydrophobic surfaces is also reported in some studies. “Late pinning mode” is observed on smooth hydrophobic surfaces<sup>25,26</sup> leading to an inner coffee-ring deposit having the diameter smaller than the initially wetted diameter. Furthermore, it was observed that an addition of salt increases the radius of the structure.<sup>26</sup> Morphological transitions and buckling were also observed in a NP laden sessile droplet on a hydrophobic substrate.<sup>27</sup>

Apart from the coffee-ring, uniform deposition, and clump of NPs, various other patterns are formed upon evaporation of the nanofluid droplet. Drying nanofluid droplet containing ZnO nanorods leads to the formation of a uniform film on a glass surface with the structures of the 3D fiber network within the dried film, which is very different from the coffee-ring effect.<sup>28</sup> Spherical magnetite NPs lead to the formation of a dendrite-like self-assembled structure.<sup>29</sup> Copper-water and graphite-water based nanofluids lead to the formation of branched fractal-like structures on a silicon wafer.<sup>30,31</sup> Spoke patterns are formed upon evaporation from a sphere-on-flat geometry.<sup>32</sup>

Anisotropic particles are found to behave differently than the spherical particles. The direction of the crack formed after

drying of colloidal suspension varies with the particle shape anisotropy.<sup>33</sup> It is reported that the spherical particles lead to the formation of a coffee-ring while ellipsoidal particles or a mixture of ellipsoidal and spherical particles of diameter less than the minor axis of an ellipse lead to the formation of a uniform deposit.<sup>34</sup> In a recent study of Agthe *et al.*<sup>35</sup> they reported that the self-assembly of iron oxide nanocubes occurs in three stages: first, the convection-driven deposition of NPs at the edge of the drying droplet, i.e., the coffee-ring effect; as the evaporation progresses, dendritic growth (or fingering) in a transition regime; and finally spontaneous diffusion-controlled formation of mesocrystals in the centre region. Xie *et al.*<sup>36</sup> studied two-stage evaporation of droplet containing gold nanorods. The fast evaporation offers the pinned edge (coffee-ring) preventing the shrinkage of the droplet area, and then, the slow evaporation in solvent saturated atmosphere forms large area self-assembled monolayer arrays. The information from above studies is insufficient to provide a good understanding of the effect of shape and size of NPs on their self-assembly during evaporation. Thus, molecular simulation methodologies are apt to investigate such systems.

The first molecular dynamics (MD) simulation study for evaporation was reported by Long *et al.*<sup>37</sup> in 1996, where they studied the evaporation of an argon drop on a surface. Since then, various MD studies have been performed for evaporation of the Lennard-Jones (LJ) liquid,<sup>38</sup> sodium drop,<sup>39</sup> argon nanodroplet in its own vapor,<sup>40</sup> vaporization and condensation of an ultra-thin liquid argon layer on a surface,<sup>41</sup> and wetting and evaporation of argon nanodroplets on smooth and rough substrates.<sup>42</sup> In addition, the evaporation of Lennard-Jones fluid<sup>43</sup> on hydrophilic and hydrophobic substrates<sup>44</sup> and on rough and smooth surfaces,<sup>45</sup> the effect of the contact line curvature in the case of cylindrical and spherical drops<sup>46</sup> and pinning of the contact line on a chemically modified heterogeneous surface<sup>47</sup> have been studied using MD simulations. Evaporation flux distribution of drops on hydrophilic and hydrophobic flat surfaces is studied for three different evaporation modes such as the diffusion dominant mode, the substrate heating mode, and the environment heating mode.<sup>48</sup> Evaporation of water droplets on a platinum surface in the presence of electric field<sup>49</sup> and self-assembly of magnetic NP in an evaporating solvent have also been studied.<sup>50</sup> MD simulations are also applied for the evaporating nanofluid droplet laden with spherical particles to study the effect of chemical anisotropy and charge on the self-assembled structure of nanoparticles.<sup>51</sup> The role of spherical nanoparticle solubility and the solvent evaporation rate is analyzed on the pattern formed on the surface.<sup>52</sup>

The effect of hydrodynamic retardation and inter-particle interactions on the self-assembly in a drying droplet containing suspended solid particles is also studied using the Monte Carlo method. The model explains the formation of the coffee-ring pattern even without accounting for the radial flows towards the three phase contact line. The structure of the drying patterns and their dependence on inter-particle interactions and concentration of particles are discussed.<sup>53</sup> The coarse-grained lattice model considering

both evaporative convection and the Brownian motion results in the formation of different patterns depending on the interplay of these parameters. The ring-like pattern is formed when the convective potential dominates the interaction of particles.<sup>54</sup> The finite element numerical model based studies have been used to study the pattern formation during drying.<sup>55</sup>

The above literature review points out that different methodologies have been used to study the evaporation of nanofluids using both experiments and simulations. Still, there are questions which are not well addressed, such as (a) the effect of substrate wettability on the self-assembled structure of nanoparticles and (b) the role of shape and size of NPs on the self-assembled structure. In this direction, we have considered four different shapes of NPs of varying sizes. In order to address the effect of the solvophobic/solvophilic surface, we have varied the NP-surface and solvent-surface interactions using molecular dynamics simulations. In Sec. II, we have described the model and the details of the simulation. Section III presents the results and discussion, and finally, the conclusions are presented in Sec. IV.

## II. MODEL AND SIMULATION DETAILS

We have used molecular dynamics (MD) simulations to study the effect of size and shape of the nanoparticle and solvent-surface ( $\epsilon_{fs}$ ) and NP-surface ( $\epsilon_{ns}$ ) interaction strengths on the structure of the deposit formed upon evaporation of the nanoparticle (NP) laden nanofluid droplet on a surface maintained at a constant temperature. The system consists of a hemispherical nanofluid droplet, placed on top of a solid surface, located at the bottom of a simulation box, as shown in Fig. 1. For simplicity, the solid surface, solvent, and NPs are all represented using Lennard-Jones (LJ) atoms. The interaction between all the beads is given by the LJ 12-6 potential energy function, as defined in Eq. (1). Where  $\epsilon$ ,  $\sigma$ , and  $r$  are

the interaction strength, the closest distance of approach, and the distance between two particles, respectively. Equation (2) represents the truncated and shifted function to make Eq. (1) continuous at the cutoff ( $r_c$ ), and the expression  $U_{LJ\_shift}(r)$  is zero for  $r > r_c$ ,

$$U_{LJ}(r) = 4\epsilon \left[ \left( \frac{\sigma}{r} \right)^{12} - \left( \frac{\sigma}{r} \right)^6 \right], \quad (1)$$

$$U_{LJ\_shift}(r) = U_{LJ}(r) - U_{LJ}(r_c), \quad \text{for } r \leq r_c. \quad (2)$$

The solvent molecule is represented as a monoatomic LJ bead. The surface consists of four layers of LJ atoms, arranged in FCC lattice with a lattice constant of  $1.9\sigma_{ff}$  and dimensions of  $150.1\sigma_{ff}$  in both  $x$  and  $y$  directions. Where  $\sigma_{ff}$  and  $\epsilon_{ff}$  are the solvent-solvent interaction parameters. Table I lists the various interaction parameters used in the simulations. The simulation box height in the  $z$  dimension is taken as  $147\sigma_{ff}$ . Different shapes (sphere, cube, triangle, and rod) of NPs are considered for the nanofluids. NPs are represented using the coarse-grain model. Hollow spherical NPs are made by arranging atoms on the circumference of a particular radius.<sup>56</sup> Spherical NPs of outer diameter  $D = 4\sigma_{ff}$ ,  $5\sigma_{ff}$ , and  $6\sigma_{ff}$  have 40, 62, and 90 number of beads, respectively. Hollow cubic NPs are made by putting beads on the surface of the cube. The cubic NPs of outer edge length  $L = 4\sigma_{ff}$ ,  $5\sigma_{ff}$ , and  $6\sigma_{ff}$  have 56, 98, and 152 number of beads, respectively, and these beads are arranged in a square lattice. Triangular NPs of edge length  $L = 4\sigma_{ff}$ ,  $5\sigma_{ff}$ , and  $6\sigma_{ff}$  are made by arranging beads in a triangular lattice. The rod shaped NPs of length  $L = 4\sigma_{ff}$ ,  $5\sigma_{ff}$ , and  $6\sigma_{ff}$  are simply made by putting LJ beads in a liner fashion. The distance between the beads is kept as  $1\sigma_{ff}$  in a cube, triangle, and rod shaped NPs. Different shapes of NPs are shown in Fig. 1(b). The initial volume percentage of NPs in the solvent is fixed at  $\sim 4.5\%$  for all the shapes. All the parameters mentioned are in reduced units. The distance, energy, and mass are reduced by  $\sigma_{ff}$ ,  $\epsilon_{ff}$  of solvent-solvent interaction, and the mass of the solvent atom, respectively.

MD simulations are performed in four steps: first the nanofluid is equilibrated at a reduced temperature ( $T$ ) of 0.67 (temperature is reduced by  $\epsilon_{ff}/k_B$ ) in an NPT ensemble, then the equilibrated box containing NPs and the solvent is placed on the solid surface, and the complete system is equilibrated at  $T = 0.67$  for a time of  $10000\tau$ . Where  $\tau = \sigma_{ff}\sqrt{m_{ff}/\epsilon_{ff}}$  is the unit of time. The third step involves equilibrating the system at  $T = 0.83$  for  $10000\tau$ . The final step involves the evaporation of the solvent. The evaporation starts  $20000\tau$  after the drop of nanofluid is placed on the surface. For evaporating the solvent in MD simulations, a region is defined at the top of a

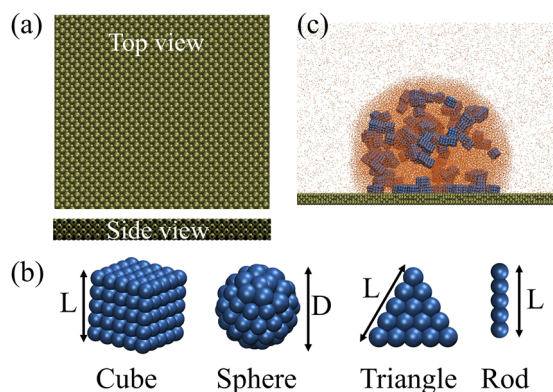


**FIG. 1.** (a) Snapshots showing the top view and side view (showing 4 layers) of the surface. (b) Different shapes of NPs used in simulations, cube, sphere, triangle, and rod, each having length ( $L$ ) or diameter ( $D$ ), which in the case of sphere is equal to 5. (c) Simulation box showing a nanofluid droplet on a surface, in equilibrium with its vapor.

**TABLE I.** Set of parameters used for simulations in reduced units.

Interacting beads	$\epsilon/\epsilon_{ff}$	$\sigma/\sigma_{ff}$
Surface-surface	10.0	1.2
Nanoparticle-nanoparticle	1.0	1.0
Nanoparticle-solvent	1.0	1.0
Solvent-surface	0.4, 0.7, 0.9	1.1
Nanoparticle-surface	0.4, 0.7, 0.9	1.1

simulation box (top  $15\sigma_{\text{ff}}$  units of length), and the solvent atoms are removed only from that region. The solvent is evaporated at a rate such that 1 solvent particle is removed every 50 simulation steps from that region, and if the region has less number of solvent particles, then all the solvent particles in that region are removed. The simulation is performed for  $50\,000\tau$ , which includes the evaporation of all the solvents, and once the solvent has evaporated, the simulation continues to characterize the formed structures. Throughout the evaporation, only the temperature of the substrate is maintained at  $T = 0.83$ , and the lowest layer of the surface is kept fixed, while the above three layers are flexible to mimic the evaporation process in substrate heated mode. The second and third steps of simulation are performed using the NVT ensemble. The Berendsen thermostat is chosen to control the temperature with a coupling time of  $0.25\tau$ . The NPs are kept rigid during the simulations, and the velocity-Verlet algorithm is used for integrating the equations of motion. The time step used in the simulations is  $0.0025\tau$ , and the cutoff ( $r_c$ ) is  $4.4\sigma_{\text{ff}}$ . Simulations are performed using the LAMMPS package,<sup>57</sup> and all the snapshots are generated using VMD (Visual Molecular Dynamics), a molecular visualization program.<sup>58</sup>

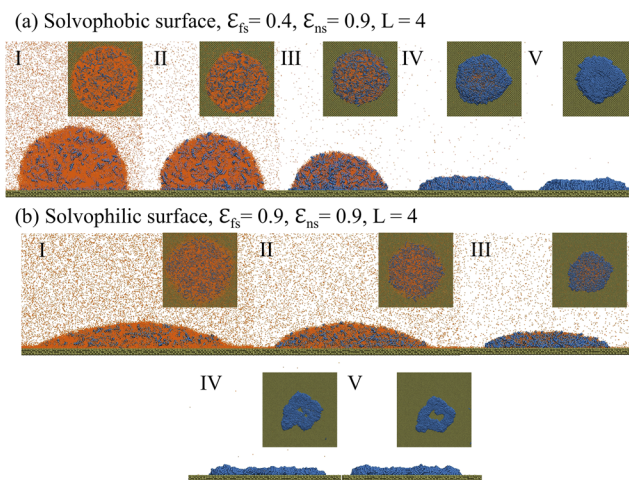
### III. RESULTS AND DISCUSSIONS

We have considered the effect of four factors, namely, solvent–surface and nanoparticle–surface interaction strengths and size and shape of nanoparticles, on the structure of the NP deposit formed upon evaporation of the solvent from the nanofluid droplet. First, we consider the evaporation of the nanofluid droplet consisting of rod shaped NPs and look into the effect of changing nature of the surface from solvophobic to solvophilic on the shape of the nanofluid droplet. Figure 2(a) shows the shape of the nanofluid droplet containing rod shaped NPs, on the solvophobic surface ( $\epsilon_{\text{fs}} = 0.4$ ,  $\epsilon_{\text{ns}} = 0.9$ , and  $L = 4$ ). The images I, II, III, IV, and V show the snapshots at different times  $0\tau$ ,  $5\,000\tau$ ,  $10\,000\tau$ ,  $15\,000\tau$ , and  $50\,000\tau$ , respectively, since the start of evaporation in step 4. It is observed that as the evaporation progresses, the amount of solvent in the nanodrop decreases along with the reduction in the contact angle of the nanodrop on the surface.

Figure 2(b) shows the shape of the nanofluid droplet, containing rod shaped NPs, on the solvophilic surface ( $\epsilon_{\text{fs}} = 0.9$ ,  $\epsilon_{\text{ns}} = 0.9$ , and  $L = 4$ ). In the case of a solvophilic surface, the drop spreads relatively more on the surface, increasing the contact area with the surface as compared to the solvophobic surface. This increase in the contact area increases the heat transfer from the surface to the solvent atoms which can be established from the higher number of solvent molecules in the vapor state. This increase in solvent molecules in the vapor phase is evident in Fig. 3 and is discussed in Sec. III A. The final structure formed by the NPs during evaporation will be discussed in Sec. III B.

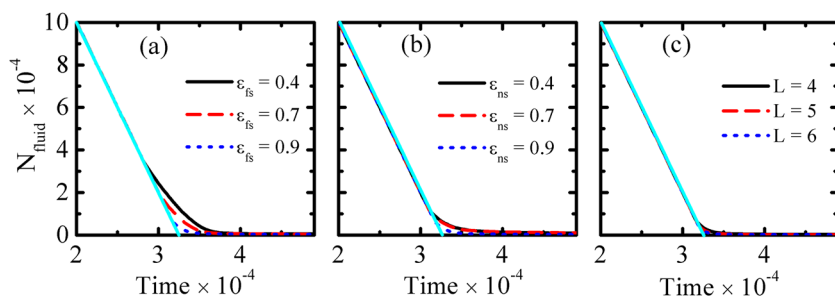
#### A. Effect on the evaporation rate

Figure 3 shows the total number of solvent atoms ( $N_{\text{fluid}}$ ) present in the system (including liquid and vapor phases), as a



**FIG. 2.** (a) Snapshots showing the shape of the nanofluid droplet, with rod shaped NPs, with time during evaporation on the solvophobic surface ( $\epsilon_{\text{fs}} = 0.4$ ,  $\epsilon_{\text{ns}} = 0.9$ , and  $L = 4$ ). (b) Snapshots showing the shape of the nanofluid droplet, with rod shaped NPs, with time during evaporation on the solvophilic surface ( $\epsilon_{\text{fs}} = 0.9$ ,  $\epsilon_{\text{ns}} = 0.9$ , and  $L = 4$ ), having different images I, II, III, IV, and V, which show the snapshots at different times  $0\tau$ ,  $5\,000\tau$ ,  $10\,000\tau$ ,  $15\,000\tau$ , and  $50\,000\tau$ , respectively, since the start of evaporation in step 4. Snapshots in the top right corner of each image are the top view, and the bottom row shows the side view of the nanofluid drop at different evaporation times. The green, orange, and blue colours represent the surface, solvent, and NPs, respectively.

function of evaporation time. As mentioned earlier, the evaporation rate of the solvent is maintained by removing 1 solvent particle every 50 simulation steps. This rate is represented by a cyan line in all the plots of Fig. 3. It is observed that during the evaporation of a nanofluid droplet, this rate shows some variation mainly in the later stage of evaporation with the change in the various parameters. This is clearly evident from Fig. 3, where the number of solvent atoms present in the system ( $N_{\text{fluid}}$ ), at a later stage of evaporation, is more than that corresponding to the fixed rate (see the cyan line), thereby reducing the actual evaporation rate. In general, there are two regions, one in which the constant evaporation rate is followed (the portion of the curves which overlaps with the cyan line) and the other in which the rate decreases due to factors influencing the evaporation. The reduction in evaporation rate varies with different factors such as  $\epsilon_{\text{fs}}$ ,  $\epsilon_{\text{ns}}$ , and size of NPs. Figure 3(a) shows the effect of changing  $\epsilon_{\text{fs}}$  on the evaporation rate of a nanofluid droplet containing rod shaped NPs of  $L = 4$  and with  $\epsilon_{\text{ns}} = 0.9$ . The evaporation rate decreases with the decreasing  $\epsilon_{\text{fs}}$ . The time taken to reach  $N_{\text{fluid}}$  close to zero is high for low  $\epsilon_{\text{fs}}$  values. For  $\epsilon_{\text{fs}} = 0.9$ , there is an insignificant change in the evaporation rate, compared to the cyan line, while for lower values of  $\epsilon_{\text{fs}}$ , the rate decreases with decreasing  $\epsilon_{\text{fs}}$ . This behavior of  $N_{\text{fluid}}$  with the changing  $\epsilon_{\text{fs}}$  is due to the fact that at low  $\epsilon_{\text{fs}}$ , the surface acts as solvophobic for the nanofluid droplet, and thus, its contact area on the surface is less compared to the case of high  $\epsilon_{\text{fs}}$ , where the surface behaves as solvophilic. Due to the less contact area at low  $\epsilon_{\text{fs}}$ , less energy is transferred to the nanofluid from the surface



**FIG. 3.** Number of solvent atoms ( $N_{\text{fluid}}$ ) present in the system as a function of evaporation time for rod shaped NPs. (a)  $L = 4$ ,  $\epsilon_{\text{ns}} = 0.9$ , and with variable  $\epsilon_{\text{fs}}$ . (b)  $L = 4$ ,  $\epsilon_{\text{fs}} = 0.9$ , and with variable  $\epsilon_{\text{ns}}$ . (c)  $\epsilon_{\text{fs}} = 0.9$ ,  $\epsilon_{\text{ns}} = 0.9$ , and with different values of the size of NPs ( $L$ ). The cyan line represents the  $N_{\text{fluid}}$  due to the evaporation rate fixed during the simulations.

and, hence, less solvent evaporates in comparison to the high  $\epsilon_{\text{fs}}$  value. Furthermore, if we look into the effect of changing  $\epsilon_{\text{ns}}$  at  $\epsilon_{\text{fs}} = 0.9$  for rod shaped nanoparticles of  $L = 4$ , we find that all the curves for different  $\epsilon_{\text{ns}}$  values overlap as shown in Fig. 3(b). This indicates that at a high  $\epsilon_{\text{fs}}$  value, there is no effect of  $\epsilon_{\text{ns}}$  in reducing the evaporation rate. The effect of size on  $N_{\text{fluid}}$  is shown in Fig. 3(c) for  $\epsilon_{\text{fs}} = 0.9$  and  $\epsilon_{\text{ns}} = 0.9$ . It is evident that the size does not show any effect on  $N_{\text{fluid}}$ . It signifies that  $\epsilon_{\text{fs}}$  is the dominant factor in influencing the evaporation rate, and the effect of other factors is suppressed at  $\epsilon_{\text{fs}} = 0.9$ .

## B. Self-assembled structures of NPs

Figure 4 presents the self-assembled structures of rod shaped NPs formed on the surface as a result of evaporation of the solvent from the nanofluid droplet. Figure 4(a) shows the structures for  $\epsilon_{\text{fs}} = 0.4$  and varying  $\epsilon_{\text{ns}}$  and size. At  $\epsilon_{\text{fs}} = 0.4$ , we observe that at a low value of  $\epsilon_{\text{ns}} = 0.4$ , a hemispherical clump is formed on the surface upon evaporation of the solvent. As the  $\epsilon_{\text{ns}}$  is changed to 0.7 and 0.9, the hemispherical pattern flattens on the surface. This structure is observed for all the different sizes of NPs. Figure 4(b) presents the structure of NPs for  $\epsilon_{\text{fs}} = 0.7$ , which is similar in nature as observed for  $\epsilon_{\text{fs}} = 0.4$ , except that at  $\epsilon_{\text{ns}}$  of 0.9, we observe an onset of the coffee-ring effect. Figure 4(c) shows the results for a solvophilic surface with  $\epsilon_{\text{fs}} = 0.9$ , different NP size ( $L$ ), and  $\epsilon_{\text{ns}}$  values. For  $L = 4$ , the pattern of NPs changes from a hemispherical clump to a flat clump and then to a ring, with increasing  $\epsilon_{\text{ns}}$ . For  $L = 5$ , the structure is not hemispherical at  $\epsilon_{\text{ns}} = 0.4$ , and the ring structure is formed at  $\epsilon_{\text{ns}} = 0.7$ , which breaks into a small number of

clusters at  $\epsilon_{\text{ns}} = 0.9$ . At a higher size of the NP,  $L = 6$ , we do not see a single cluster of NPs at all values of  $\epsilon_{\text{ns}}$ , rather a distorted ring-like structure of NPs is formed. The number of small clusters increases with the increase in the  $\epsilon_{\text{ns}}$  value. It is apparent from Fig. 4(c) that the tendency to form a ring increases with the increase in the size of NPs, which is also observed experimentally.<sup>18</sup> It is also observed that the size of NPs at which the ring formation initiates varies with  $\epsilon_{\text{ns}}$ .

We have presented the different structures obtained after evaporating the solvent from the nanofluid droplet. It is intriguing to understand the reasons behind the formation of such structures. In order to explain the existence of these structures and to provide the reason for different structures formed, we have attempted to gain insight into some structural and thermodynamic properties. We have separately discussed the effect of  $\epsilon_{\text{fs}}$ ,  $\epsilon_{\text{ns}}$ , and size of NPs on various properties. For the sake of brevity, we present the data for which some structural changes occur upon changing one of the parameters. In order to analyze the effect of  $\epsilon_{\text{fs}}$ , we have taken structures corresponding to  $L = 4$  and  $\epsilon_{\text{ns}} = 0.9$ . Similarly, we have considered structures corresponding to  $L = 4$  and  $\epsilon_{\text{fs}} = 0.9$  to understand the effect of  $\epsilon_{\text{ns}}$ . The effect of size is explained using structures corresponding to  $\epsilon_{\text{fs}} = 0.9$  and  $\epsilon_{\text{ns}} = 0.9$ .

## C. Pair energy

First, we have calculated the pair energies per NP during evaporation. The pair energy is obtained by calculating the van der Waals contribution between all the nanoparticles ( $E_{\text{NP-NP}}$ )

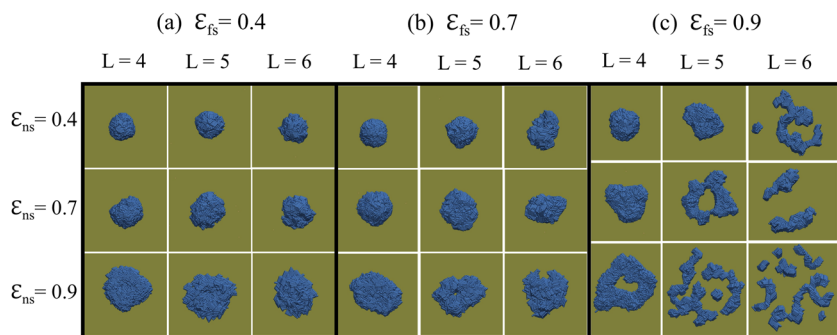


**FIG. 4.** Snapshots illustrating the shape of deposits formed on the surface upon evaporation of the solvent from the nanofluid droplet, containing rod shaped nanoparticles of different sizes ( $L$ ) and for different nanoparticle–surface ( $\epsilon_{\text{ns}}$ ) interaction strengths. (a)  $\epsilon_{\text{fs}} = 0.4$ , (b)  $\epsilon_{\text{fs}} = 0.7$ , and (c)  $\epsilon_{\text{fs}} = 0.9$ .

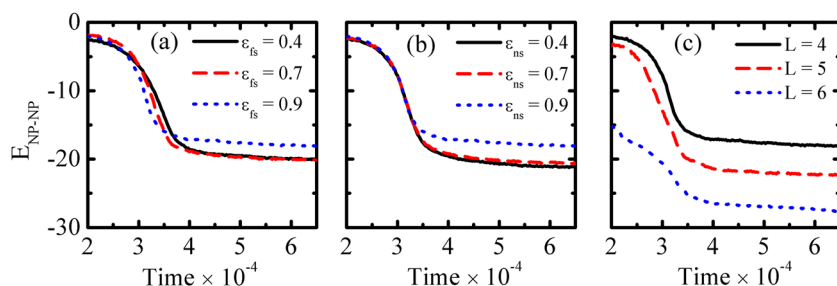


**FIG. 5.** Pair energy per nanoparticle between nanoparticle–nanoparticle  $E_{\text{NP-NP}}$  as a function of evaporation time for rod shaped NPs. (a)  $L = 4$ ,  $\epsilon_{\text{ns}} = 0.9$ , and showing the effect of  $\epsilon_{\text{fs}}$ . (b)  $L = 4$ ,  $\epsilon_{\text{fs}} = 0.9$ , and showing the effect of  $\epsilon_{\text{ns}}$ . (c)  $\epsilon_{\text{fs}} = 0.9$  and  $\epsilon_{\text{ns}} = 0.9$ , showing the effect of size of NPs ( $L$ ).

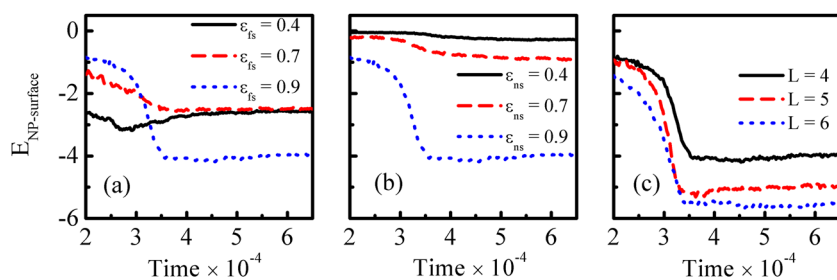
or nanoparticles with the surface ( $E_{\text{NP-Surface}}$ ) using Eqs. (1) and (2). The pair energies  $E_{\text{NP-NP}}$  and  $E_{\text{NP-Surface}}$  are shown in Figs. 5 and 6, respectively. During evaporation, the behavior of pair energies changes. In the initial region, the decrease in energy is very slow, and as the amount of solvent decreases with evaporation, the NPs come close to each other and to the surface leading to a rapid decrease in the pair energy per NP. Once a considerable amount of the solvent has evaporated, and NPs have attained their equilibrium positions with respect to each other and with the surface, then a very small decrease in the pair energy is observed. This small decrease is due to the rearrangement of particles to attain minimum energy further. The  $E_{\text{NP-NP}}$  shown in Fig. 5 is observed to decrease with time during evaporation. For the case of rod shaped NPs of  $L = 4$  and  $\epsilon_{\text{ns}} = 0.9$ , as shown in Fig. 5(a), the values at the initial states are almost similar for different  $\epsilon_{\text{fs}}$  values, although at the final state, after the evaporation, a higher value of  $E_{\text{NP-NP}}$  is observed for  $\epsilon_{\text{fs}} = 0.9$ . At  $\epsilon_{\text{fs}} = 0.4$  and  $0.7$ , the NPs form a single cluster (see Fig. 4) and maximize their contact with each other while at  $\epsilon_{\text{fs}} = 0.9$ , NPs self-assemble into a ring structure leading to less number of contacts between NPs, and hence, the  $E_{\text{NP-NP}}$  is high. Figure 5(b) shows the effect of  $\epsilon_{\text{ns}}$  at  $\epsilon_{\text{fs}} = 0.9$  and  $L = 4$ . The  $E_{\text{NP-NP}}$  values of the final structure of NPs increase with the increasing  $\epsilon_{\text{ns}}$ . To study the effect of size, we have fixed  $\epsilon_{\text{fs}} = 0.9$  and  $\epsilon_{\text{ns}} = 0.9$  and varied  $L = 4, 5$ , and  $6$ . For NPs of different sizes, the initial energies are not the same, and hence, we look at the difference in the energies of initial and final states. The difference in energies increases as the size of NPs decreases. From the  $E_{\text{NP-NP}}$  plots, we can summarize that for the ring structure, the  $E_{\text{NP-NP}}$  values are higher in comparison to the clump of NPs formed on evaporation of the nanofluid droplet.

Figure 6 shows the pair energy per NP as a result of NP–surface interaction. It is observed that  $E_{\text{NP-Surface}}$  decreases

with the evaporation, though the  $E_{\text{NP-Surface}}$  values at the start of evaporation are different for all the cases. Figure 6(a) shows the effect of  $\epsilon_{\text{fs}}$  on the  $E_{\text{NP-Surface}}$  for  $L = 4$  and  $\epsilon_{\text{ns}} = 0.9$ . The decrease in energy upon evaporation is higher for the high value of  $\epsilon_{\text{fs}}$ . At  $\epsilon_{\text{fs}} = 0.4$  and  $0.7$  (see also Fig. 4), the NPs form a single cluster, and at  $\epsilon_{\text{fs}} = 0.9$ , the NPs form a ring. It is found that the number of NP beads interacting with the surface is large for the ring structure than the single cluster, and hence, the  $E_{\text{NP-Surface}}$  is low. Thus, for the case of formation of a clump of NPs,  $E_{\text{NP-Surface}}$  is high; whereas, if the ring structure is formed,  $E_{\text{NP-Surface}}$  decreases. For  $\epsilon_{\text{fs}} = 0.4$  and  $0.7$ , insignificant differences in the  $E_{\text{NP-Surface}}$  values are seen after evaporation as the formed structures are almost the same in both the cases. Furthermore, we look into the effect of  $\epsilon_{\text{ns}}$  at  $\epsilon_{\text{fs}} = 0.9$  and  $L = 4$  which is shown in Fig. 6(b). The effect of  $\epsilon_{\text{ns}}$  is akin to that seen for  $\epsilon_{\text{fs}}$ . The  $E_{\text{NP-Surface}}$  decreases as the  $\epsilon_{\text{ns}}$  increases. The ring structure corresponds to the lower  $E_{\text{NP-Surface}}$  compared to the clump of NPs. The effect of the size of NPs on  $E_{\text{NP-Surface}}$  is shown in Fig. 6(c) for  $\epsilon_{\text{fs}} = 0.9$  and  $\epsilon_{\text{ns}} = 0.9$ . The value of  $E_{\text{NP-Surface}}$  decreases with increasing size of NPs. From the  $E_{\text{NP-Surface}}$  analysis, we can summarize that for the ring structure, the  $E_{\text{NP-Surface}}$  is lower compared to the clump of NPs formed on evaporation of the nanofluid droplet.

#### D. Excess entropy due to nanoparticle–nanoparticle

We have also calculated the contribution of the nanoparticle–nanoparticle to the excess entropy,  $S_{\text{NP-NP}}$  during evaporation, to study the relative stability of the self-assembled structures. We have considered the same set of structures as used for pair energy. The excess entropy is calculated within the two-body approximation,<sup>59,60</sup> using the equation



**FIG. 6.** Pair energy per nanoparticle between the nanoparticle–surface  $E_{\text{NP-Surface}}$  as a function of evaporation time for rod shaped NPs. (a)  $L = 4$ ,  $\epsilon_{\text{ns}} = 0.9$ , and showing the effect of  $\epsilon_{\text{fs}}$ . (b)  $L = 4$ ,  $\epsilon_{\text{fs}} = 0.9$ , and showing the effect of  $\epsilon_{\text{ns}}$ . (c)  $\epsilon_{\text{fs}} = 0.9$  and  $\epsilon_{\text{ns}} = 0.9$ , showing the effect of size of NPs ( $L$ ).

$$S_{\text{NP-NP}} = -2\pi\rho \int \{g(r) \ln g(r) - (g(r) - 1)\} r^2 dr, \quad (3)$$

where  $g(r)$  is the 3D radial distribution function of NP–NP and  $\rho$  is the initial bulk density of NPs in the nanofluid.  $\rho$  is calculated for the NPs + fluid system, without the surface, using the isothermal–isobaric ensemble. The two-body approximation is highly correlated with the total excess entropy for Lennard–Jones fluids,<sup>51</sup> and it provides a reasonable estimate of the total excess entropy for the current system.<sup>59</sup> In the current study, we have considered the nanoparticle as a single object, where the beads are used to provide structure to the NPs. Thus, the internal degree of freedom is absent in the NPs. Since the internal degree of freedom of nanoparticle is not considered in the model, we do not consider any contribution of the internal degree of freedom in the entropy calculation. To study the effect of  $\epsilon_{\text{fs}}$ , we have taken structures corresponding to  $L = 4$  and  $\epsilon_{\text{ns}} = 0.9$ . Figure 7(a) presents the contribution of the nanoparticle–nanoparticle to the excess entropy  $S_{\text{NP-NP}}$  during evaporation for varying  $\epsilon_{\text{fs}}$ . It indicates that the excess entropy per NP  $S_{\text{NP-NP}}$  initially increases for all the values of  $\epsilon_{\text{fs}}$  when there is a large amount of fluid present in the system. This increase is observed due to the reorganization of NPs from disorder to order arrangement within the nanodroplet during evaporation of the solvent. This is clearly evident from Fig. S1 of the [supplementary material](#) which shows the orientation order parameter changes drastically from almost zero to a non-zero value upon evaporation. However, as the amount of fluid decreases with continued evaporation, it imposes a restriction on the movement of NPs and leads to a decrease in the randomness of the NPs, and as a consequence, the entropy decreases. The value of  $S_{\text{NP-NP}}$  is high after the evaporation for the case of the ring structure ( $\epsilon_{\text{fs}} = 0.9$ ) than the case of a single agglomerate of NPs ( $\epsilon_{\text{fs}} = 0.4$  and  $0.7$ ). Figure 7(b) shows the variation of  $S_{\text{NP-NP}}$ , as a function of  $\epsilon_{\text{ns}}$ , for  $L = 4$  and  $\epsilon_{\text{fs}} = 0.9$ . The behavior of  $S_{\text{NP-NP}}$  is similar to that observed due to changes in  $\epsilon_{\text{fs}}$ . During evaporation, the decrease in entropy is larger for  $\epsilon_{\text{ns}} = 0.4$ , and as the  $\epsilon_{\text{ns}}$  increases to  $0.7$  and  $0.9$ , the entropy is relatively high. When a clump of NPs is formed,  $S_{\text{NP-NP}}$  is lowest ( $\epsilon_{\text{ns}} = 0.4$ ), and as the NPs spread more ( $\epsilon_{\text{ns}} = 0.7$ ) or form a ring ( $\epsilon_{\text{ns}} = 0.9$ ), the entropy increases. Furthermore, we studied the effect of the size of NPs on the  $S_{\text{NP-NP}}$ , at  $\epsilon_{\text{fs}} = 0.9$  and  $\epsilon_{\text{ns}} = 0.9$  which is shown in Fig. 7(c). For  $L = 4$  and  $5$ , the  $S_{\text{NP-NP}}$  shows an initial increase and then decrease in the  $S_{\text{NP-NP}}$  values, akin to that seen in Figs. 7(a) and 7(b), and for  $L = 6$ , the entropy decreases with evaporation. The  $S_{\text{NP-NP}}$  values have a negligible change with the size for the chosen structures

as all the structures are either ring or distributed small clusters. Based on the aforementioned results, it is evident that entropy changes significantly upon change in  $\epsilon_{\text{fs}}$  or  $\epsilon_{\text{ns}}$ . It is also observed that the clump of NPs has a lowest entropy and the ring shaped structure has the highest entropy.

### E. Mean squared displacement of nanoparticles

The dynamics of NPs is greatly affected by the interaction parameters. Thus, to understand the diffusional behavior of NP upon evaporation, we have calculated the mean squared displacement (MSD) of the NPs during evaporation as a function of time ( $t$ ). MSD is calculated using the equation as follows:

$$\text{MSD}(t) = \frac{1}{N_{\text{NP}}} \sum_{i=1}^{N_{\text{NP}}} [r_i(t) - r_i(0)]^2. \quad (4)$$

Here  $N_{\text{NP}}$  is the total number of NPs in the system and  $r_i(t)$  is the position of a particular NP at time  $t$ , and  $r_i(0)$  is the position of the same NP at the start of evaporation. The shape of MSD as shown in Fig. 8 for all the systems is such that initially there is an increase while the solvent is evaporating and the NPs are rearranging themselves, and as the structure of the NPs deposit is frozen, a flat plateau is obtained. The onset of the flat region signifies that the structures formed by NPs no longer change and further negligible diffusion of the NPs occurs. It also gives an estimate of the time in which the solvent has evaporated completely.

For the case of rod shaped NPs of  $L = 4$  and  $\epsilon_{\text{ns}} = 0.9$ , for varying  $\epsilon_{\text{fs}}$  values in Fig. 8(a), the structures for  $\epsilon_{\text{fs}} = 0.4$  and  $0.7$  are very similar. Consequently, the final MSD values are close to each other and also the time taken to reach the plateau is very close.  $\epsilon_{\text{fs}} = 0.9$  shows the higher MSD value as compared to  $\epsilon_{\text{fs}} = 0.4$  and  $0.7$ . Figure 8(b) shows the MSD results for the case of  $L = 4$  and  $\epsilon_{\text{fs}} = 0.9$ , with varying  $\epsilon_{\text{ns}}$  value. It is evident that the ring-like structure at  $\epsilon_{\text{ns}} = 0.9$  is formed in lesser time, as the plateau is reached quickly. Also, the displacement of the NPs is less for a ring-like structure. Furthermore, as the  $\epsilon_{\text{ns}}$  value decreases, more time is needed to reach the plateau region, and also, the displacement of the NPs increases when a clump of NPs is formed.

To study the effect of the size, we have considered structures corresponding to  $\epsilon_{\text{fs}} = 0.9$  and  $\epsilon_{\text{ns}} = 0.9$ . The MSD of NPs decreases with increasing size of NPs, as shown in Fig. 8(c), although the time required to reach the plateau region is almost the same for all the sizes of NPs for the current set of parameters used.

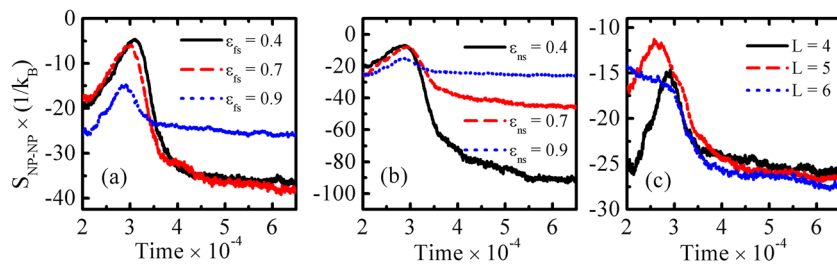


**FIG. 7.** Excess entropy contribution due to nanoparticle–nanoparticle  $S_{\text{NP-NP}}$  as a function of evaporation time, for rod shaped NPs. (a)  $L = 4$ ,  $\epsilon_{\text{ns}} = 0.9$ , and showing the effect of  $\epsilon_{\text{fs}}$ . (b)  $L = 4$ ,  $\epsilon_{\text{fs}} = 0.9$ , and showing the effect of  $\epsilon_{\text{ns}}$ . (c)  $\epsilon_{\text{fs}} = 0.9$  and  $\epsilon_{\text{ns}} = 0.9$ , showing the effect of size of NPs ( $L$ ).

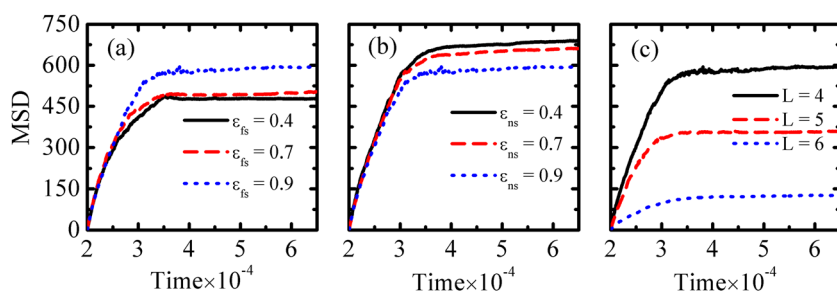


**FIG. 8.** Mean square displacement of nanoparticles as a function of evaporation time, for rod shaped NPs. (a)  $L = 4$ ,  $\epsilon_{ns} = 0.9$ , and showing the effect of  $\epsilon_{fs}$ . (b)  $L = 4$ ,  $\epsilon_{fs} = 0.9$ , and showing the effect of  $\epsilon_{ns}$ . (c)  $\epsilon_{fs} = 0.9$  and  $\epsilon_{ns} = 0.9$ , showing the effect of size of NPs ( $L$ ).

### F. Effect of shape

We have also investigated the effect of different shapes of nanoparticles: spheres, triangles, and cubes. Figure 9 shows the different self-assembled structure of spherical NPs. At  $\epsilon_{fs} = 0.4$  [see Fig. 9(a)], all the structures are hemispherical clumps, and there is no change in the formed structure with changing  $\epsilon_{ns}$  or size. As the  $\epsilon_{fs}$  is increased to 0.7, as shown in Fig. 9(b), NPs spread more on the surface as compared to  $\epsilon_{fs} = 0.4$ , still forming a clump of NPs, and no change in the structures is observed with changing  $\epsilon_{ns}$  or size. At a higher fluid–surface interaction,  $\epsilon_{fs} = 0.9$ , change in the structure is noticed with increasing  $\epsilon_{ns}$  values, as shown in Fig. 9(c).

For a fixed size of NPs, more spreading is observed with increase in  $\epsilon_{ns}$ , leading to the formation of anisotropic structures. Increasing the size of NPs for a fixed  $\epsilon_{ns}$  also results in increased spreading of NPs on the surface and leads to the formation of monolayers. These structures are quite different from those formed by rod shaped NPs.

Figure 10 shows the structures formed by triangle and cube shaped NPs upon evaporation of the solvent. We have fixed  $\epsilon_{ns} = 0.9$  and varied size and  $\epsilon_{fs}$  values. It is evident that the two shape (triangle and cube) NPs show a considerable difference in the structure of the deposit. For triangular NPs [see Fig. 10(a)], we observe that with an increase in  $\epsilon_{fs}$  values for the different sizes of NPs, the structure of the deposit changes. At

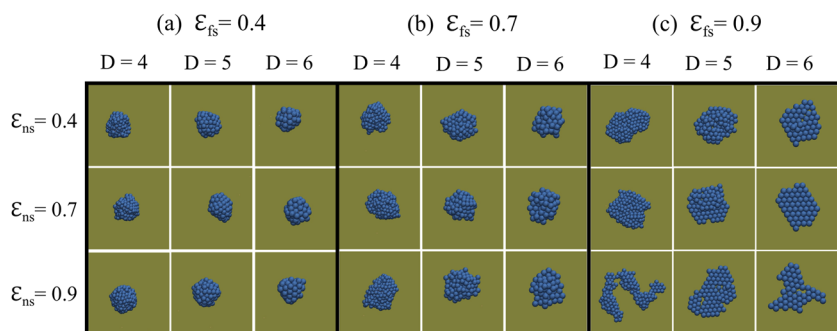


**FIG. 9.** Snapshots showing the shape of deposits formed on the surface upon evaporation of the solvent from the nanofluid droplet, containing spherical nanoparticles of different sizes ( $D$ ) and nanoparticle–surface ( $\epsilon_{ns}$ ) interaction strengths. (a)  $\epsilon_{fs} = 0.4$ , (b)  $\epsilon_{fs} = 0.7$ , and (c)  $\epsilon_{fs} = 0.9$ .

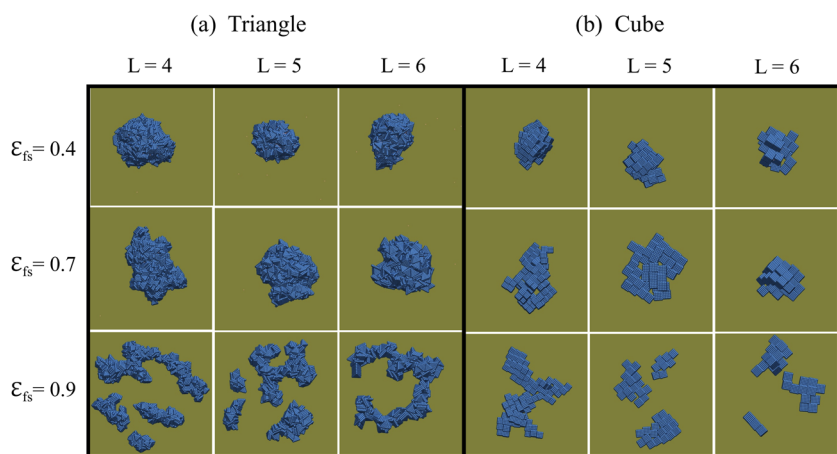


**FIG. 10.** Snapshots showing the shape of deposits formed on the surface upon evaporation of the solvent from the nanofluid droplet, with  $\epsilon_{ns} = 0.9$  and varying size and  $\epsilon_{fs}$  for (a) triangular NPs and (b) cubic NPs.

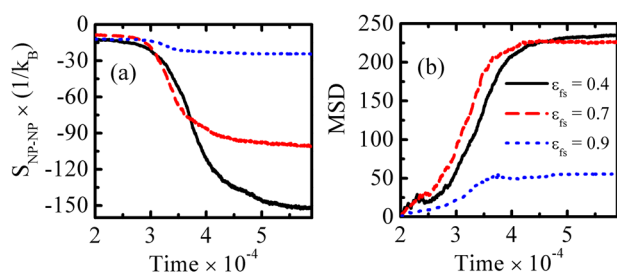


**FIG. 11.** (a) Excess entropy contribution due to nanoparticle–nanoparticle  $S_{NP-NP}$  as a function of evaporation time, for triangle shaped NPs,  $L = 4$ ,  $\epsilon_{ns} = 0.9$ , and varying  $\epsilon_{fs}$ . (b) Mean square displacement (MSD) of nanoparticles as a function of evaporation time, for triangle shaped NPs,  $L = 4$ ,  $\epsilon_{ns} = 0.9$ , and varying  $\epsilon_{fs}$ .

$\epsilon_{fs} = 0.4$ , particles form a clump of NPs, and the anisotropy of the clump increases at  $\epsilon_{fs} = 0.7$  for all the sizes. At  $\epsilon_{fs} = 0.9$ , the NPs show the coffee-ring effect, and the effect is clearly visible for larger size NPs. On the other hand, for all the sizes of cubes, the clump is formed at  $\epsilon_{fs} = 0.4$ . However, at  $\epsilon_{fs} = 0.7$ , the clump spreads slightly on the surface, which further spreads at  $\epsilon_{fs} = 0.9$  leading to the formation of smaller clusters.

In total, we have studied four different shapes of the NPs and found several structures of the NPs deposited upon evaporation. For the different shapes of NPs, the behavior of  $E_{NP-NP}$  and  $E_{NP-Surface}$  is the same during evaporation, while  $S_{NP-NP}$  shows some differences with the change in the shape of the NPs. Figure 11(a) presents the effect of  $\epsilon_{fs}$  on the  $S_{NP-NP}$  values for triangular NPs with  $\epsilon_{ns} = 0.9$  and  $L = 4$ . In the case of triangular NPs, we do not observe an initial increase in the  $S_{NP-NP}$  as in Fig. 7 for rod shaped NPs. The trend of the values such that  $S_{NP-NP}$  increases with the increase in  $\epsilon_{fs}$  is maintained with the change in shape.

We also observe slight differences in the MSD values with the change in  $\epsilon_{fs}$ , for triangular NPs interacting with  $\epsilon_{ns} = 0.9$  and  $L = 4$ . Here the ring structure is formed in lesser time for  $\epsilon_{fs} = 0.9$ , as the plateau in MSD is reached quickly, and also, the displacement of the NPs is less. As the  $\epsilon_{fs}$  values decrease, the displacement of the NPs increases. This behavior of MSD is also observed for other sizes of triangular NPs. In fact, this is the general behavior when the shape of the deposit varies from the hemispherical cluster to ring.

#### IV. CONCLUSIONS

We have presented a molecular dynamics study to understand the self-assembly of nanoparticles upon the evaporating nanofluid droplet on a surface. Various factors such as the size of NPs, shape of NPs, solvent–surface and nanoparticle–surface interaction strengths are responsible for different self-assembled structures of NPs. The solvophobic surface is responsible for the formation of a clump of NPs, while the solvophilic surface leads to the formation of different structures such as the hemispherical clump, monolayer, and ring shapes from the NPs. High nanoparticle–surface interaction strength is responsible for more spreading of NPs on the surface. The size of NPs does not play any role at low  $\epsilon_{fs}$  values

and always form a cluster of NPs for all the different shapes studied. At high  $\epsilon_{fs}$ , the small size NPs tend to form a clump while the larger size NPs have more tendency to show the coffee-ring effect. For the same interaction parameters, different shapes of NPs form different structures.

In general, the distinct feature of the ring shape structure is explained by the lower NP–surface pair energies and high NP–NP excess entropy as compared to a clump of NPs. A transition from disordered to ordered arrangement is observed for rod shaped NPs during evaporation of the solvent. The MSD of NPs is least for the ring shaped structure, and it increases as the hemispherical clump is formed.

#### SUPPLEMENTARY MATERIAL

See supplementary material for the explanation of the initial increase observed in the nanoparticle–nanoparticle excess entropy in Fig. 7 for the rod shaped nanoparticles with the help of orientation order parameter.

#### ACKNOWLEDGMENTS

This work was supported by the Science and Engineering Research Board, Department of Science and Technology (SERB–DST), Government of India. The computational resources are provided by the HPC cluster of the Computer Centre (CC), Indian Institute of Technology Kanpur.

#### REFERENCES

- 1 H. Wei et al., *NPG Asia Mater.* **9**, e395 (2017).
- 2 E. L. Talbot et al., *ACS Appl. Mater. Interfaces* **6**, 9572 (2014).
- 3 N. E. Makori et al., *Am. J. Condens. Matter Phys.* **4**, 87 (2014).
- 4 N. T. Dinh et al., *Carbon* **96**, 382 (2016).
- 5 T.-S. Wong et al., *Anal. Chem.* **83**, 1871 (2011).
- 6 T. Maul et al., *J. Bionic Eng.* **10**, 65 (2013).
- 7 J. Jeong et al., *RSC Adv.* **3**, 11801 (2013).
- 8 F. S. Romanski et al., *Langmuir* **28**, 3756 (2012).
- 9 W. Han and Z. Lin, *Angew. Chem., Int. Ed.* **51**, 1534 (2012).
- 10 R.-H. Chen, T. Phuoc, and D. Martello, *Int. J. Heat Mass Transfer* **53**, 3677 (2010).
- 11 Y. C. Kim, *Adv. Mech. Eng.* **7**, 1 (2015).
- 12 T. P. Bigioni et al., *Nat. Mater.* **5**, 265 (2006).
- 13 S. Cheng and G. S. Grest, *ACS Macro Lett.* **5**, 694 (2016).
- 14 V. Y. Shur et al., *Ferroelectrics* **476**, 47 (2015).
- 15 X. Li et al., *ACS Appl. Mater. Interfaces* **6**, 20300 (2014).
- 16 R. Bhardwaj et al., *Langmuir* **26**, 7833 (2010).
- 17 M. Parsa et al., *Langmuir* **31**, 3354 (2015).
- 18 C. H. Chon et al., *Langmuir* **23**, 2953 (2007).
- 19 P. Sun et al., *Nanotechnology* **24**, 075601 (2013).
- 20 S. Das et al., *J. Phys. Chem. Lett.* **8**, 4704 (2017).
- 21 A. Crivoi and F. Duan, *J. Phys. Chem. B* **117**, 5932 (2013).
- 22 Y. Li et al., *Sci. Rep.* **6**, 24628 (2016).
- 23 J. Zhang et al., *Phys. Rev. E* **92**, 052403 (2015).
- 24 L. H. Mujawar, W. Norde, and A. van Amerongen, *Analyst* **138**, 518 (2013).
- 25 S.-Y. Lin, K.-C. Yang, and L.-J. Chen, *J. Phys. Chem. C* **119**, 3050 (2015).
- 26 T. A. H. Nguyen, M. A. Hampton, and A. V. Nguyen, *J. Phys. Chem. C* **117**, 4707 (2013).
- 27 L. Bansal, A. Miglani, and S. Basu, *Phys. Rev. E* **93**, 042605 (2016).
- 28 H. Wu et al., *Soft Matter* **10**, 5243 (2014).
- 29 D. Reyman and R. Serrano, *Micro Nano Lett.* **9**, 613 (2014).

- <sup>30</sup>A. Crivoi and F. Duan, *J. Phys. Chem. C* **117**, 7835 (2013).
- <sup>31</sup>A. Crivoi and F. Duan, *Phys. Chem. Chem. Phys.* **14**, 1449 (2012).
- <sup>32</sup>J. Xu, J. Xia, and Z. Lin, *Angew. Chem., Int. Ed.* **46**, 1860 (2007).
- <sup>33</sup>V. R. Dugyala et al., *Sci. Rep.* **6**, 30708 (2016).
- <sup>34</sup>P. J. Yunker et al., *Nature* **476**, 308 (2011).
- <sup>35</sup>M. Agthe et al., *CrystEngComm* **16**, 1443 (2014).
- <sup>36</sup>Y. Xie et al., *Langmuir* **29**, 6232 (2013).
- <sup>37</sup>L. N. Long, M. M. Micci, and B. C. Wong, *Comput. Phys. Commun.* **96**, 167 (1996).
- <sup>38</sup>V. V. Zhakhovskii and S. I. Anisimov, *J. Exp. Theor. Phys.* **84**, 734 (1997).
- <sup>39</sup>A. P. Bhansali, Y. Bayazitoglu, and S. Maruyama, *Int. J. Therm. Sci.* **38**, 66 (1999).
- <sup>40</sup>J. H. Walther and P. Koumoutsakos, *J. Heat Transfer* **123**, 741 (2001).
- <sup>41</sup>P. Yi et al., *Int. J. Heat Mass Transfer* **45**, 2087 (2002).
- <sup>42</sup>Q. Li et al., *Chem. Phys. Lett.* **662**, 73 (2016).
- <sup>43</sup>S. Cheng et al., *J. Chem. Phys.* **134**, 224704 (2011).
- <sup>44</sup>J. Zhang, F. Leroy, and F. Müller-Plathe, *Langmuir* **29**, 9770 (2013).
- <sup>45</sup>Y.-J. Sun et al., *Front. Phys.* **12**, 126401 (2017).
- <sup>46</sup>J. Zhang, F. Leroy, and F. Müller-Plathe, *Phys. Rev. Lett.* **113**, 046101 (2014).
- <sup>47</sup>J. Zhang, F. Müller-Plathe, and F. Leroy, *Langmuir* **31**, 7544 (2015).
- <sup>48</sup>C. Xie, G. Liu, and M. Wang, *Langmuir* **32**, 8255 (2016).
- <sup>49</sup>A. Hens, G. Biswas, and S. De, *J. Chem. Phys.* **143**, 094702 (2015).
- <sup>50</sup>J. Ku et al., *J. Am. Chem. Soc.* **133**, 838 (2011).
- <sup>51</sup>W. Chen, J. Koplik, and I. Kretzschmar, *Phys. Rev. E* **87**, 052404 (2013).
- <sup>52</sup>J. Zhang et al., *J. Chem. Phys.* **146**, 114503 (2017).
- <sup>53</sup>N. I. Lebovka et al., *Phys. Rev. E* **89**, 052307 (2014).
- <sup>54</sup>N. Jung, C. S. Yoo, and P. H. Leo, *J. Phys. Chem. B* **118**, 2535 (2014).
- <sup>55</sup>R. Bhardwaj, X. Fang, and D. Attinger, *New J. Phys.* **11**, 075020 (2009).
- <sup>56</sup>E. B. Saff and A. B. J. Kuijlaars, *Math. Intell.* **19**, 5 (1997).
- <sup>57</sup>S. J. Plimpton, *J. Comput. Phys.* **117**, 1 (1995).
- <sup>58</sup>W. Humphrey, A. Dalke, and K. Schulten, *J. Mol. Graphics* **14**, 33 (1996).
- <sup>59</sup>A. Baranyai and D. J. Evans, *Phys. Rev. A* **40**, 3817 (1989).
- <sup>60</sup>T. K. Patra and J. K. Singh, *J. Chem. Phys.* **138**, 144901 (2013).
- <sup>61</sup>T. Goel et al., *J. Chem. Phys.* **129**, 164904 (2008).